Design of ultrafast all-optical PolSK DMUX based on semiconductor optical amplifiers

Hassan Kaatuzian** **and Hamed Ahmadi***

Photonics Research Lab, Electrical Engineering Department, Amirkabir University of Technology, Tehran-15914, Iran

**Corresponding author: ha.ahmadi@aut.ac.ir; ***corresponding author: hsnkato@aut.ac.ir*

Received February 28, 2012; accepted April 17, 2012; posted online August 3, 2012

A novel ultrahigh-speed all-optical demultiplexer (DMUX) with polarization-shift-keying (PolSK) modulation input signals is proposed. This design is based on four-wave mixing (FWM) in a semiconductor optical amplifier (SOA). For analyzing each amplifier, we use finite-difference method (FDM) based on solution of the traveling wave coupled equations. Using numerical simulation, the all-optical DMUX is theoretically realized at 40 Gb/s. We also study the relation between optical confinement factor and thickness of active layer of the SOA section successfully, and investigate the increasing effect of confinement factor on the DMUX optical output power. With this work, the confinement factor is increased from 0.3 to 0.48, and as a result, the output power approximately twice of its initial value is achieved. Moreover, the effects of polarization dependence of SOA on the output performance of all-optical DMUX for PolSK signal are theoretically investigated in detail.

OCIS codes: 190.4380, 230.3750, 230.4480, 230.5440.

doi: 10.3788/COL201210.091902.

An all-optical demultiplexer (DMUX) is a necessary element for optical signal processing in future ultrahigh-speed optical networks. In optical communication systems, one of the important devices is the all-optical logic gate or all-optical DMUX[1,2]. Various designs of all-optical logic gates have been created and tested, and one of the best results is the setup using a semiconductor optical amplifier (SOA). SOAs are known for their nonlinear optical effects, such as four-wave mixing (FWM). In SOAs, FWM has been used as a technique for performing wavelength conversion and ultrahigh-speed response for wavelength division multiplexing (WDM) networks. FWM can also be used for all-optical logic gates and optical DMUX in high-speed transmission systems[3].

In recent years, polarization-shift-keying (PolSK) modulation, which works according to the polarization state of the light wave, has been greatly investigated due to its unique advantages[4]. PolSK modulation can become one of the new modulation methods for future optical communication systems. In past few years, SOA has been used to implement all-optical logic gates[1,4,5], both experimentally and theoretically. In the present study, we investigate the FWM effect for all-optical DMUX in SOA with PolSK modulation signals. For analyzing this model, we use the FDM method to solve traveling wave-coupled equations numerically[6]. In the following sections, we review the operational principle, theoretical model, simulation and results, and conclusion regarding this scheme.

The suggested quantum well SOA is a 1.55-μm InP-$In_{1-x}Ga_xAs_yP_{1-y}$ device (see Fig. 1). Here, x and y are the molar fractions of gallium and arsenide, respectively, in the active layer. We use the InP-$In_{0.58}Ga_{0.42}As_{0.89}P_{0.11}$ device for our simulation because of good lattice matching. This device is specifically appropriate for amplifiers in the 1 550 nm wavelength, which has very low optical loss for silica optical fibers. Pertinent geometrical and material parameters for the device under consideration were reported in Ref. [7].

In fact, the gain of a SOA depends on the polarization state of the input signals. This dependency is due to a number of factors, including the waveguide structure, the polarization-dependent nature of the antireflection coatings, and the gain material. The amplifier waveguide is characterized by two mutually orthogonal polarization modes: the TE and TM modes. When two optical pulses with different central frequencies, f_1 and f_2, are injected into the SOA simultaneously, the FWM signal is generated in the SOA at a frequency of $2f_1-f_2$[8]. Nevertheless, producing these signals depend on the polarization state. In other words, if two input signals have one polarization state, the phase conjugate signal will be produced in the output; however, if the polarization states of two input signals are perpendicular, no signal will be produced in the output.

Figure 2 shows the schematic model of the ultrahigh-speed all-optical DMUX. In this diagram, the FWM effects in the four SOAs are used for PolSK modulation signals. In this modulation, logic "1" is a given linear polarization state, and the "0" is the orthogonal state. If polarization states of two input signals are similar, the phase conjugate signal will be produced in the output[8]. Figure 2 shows that the two input signals are split by the red optical couplers (OC). Thus, the signals past

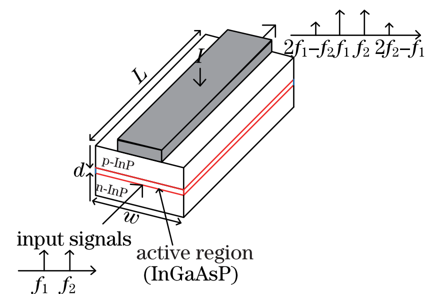

Fig. 1. Schematic crossection of homogenous buried ridge stripe SOA.

 © 2012 Chinese Optics Letters

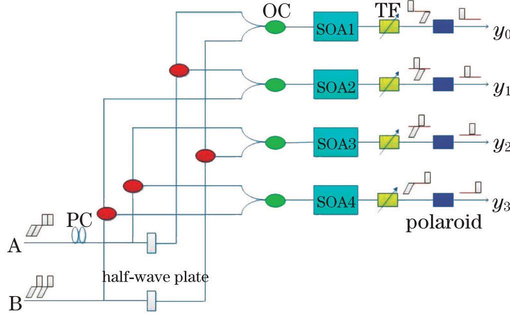

Fig. 2. Schematic diagram of the ultrafast all-optical DMUX based on FWM in SOAs with PolSK modulated signals.

the half-wave plate branches should be rotated 90° with regards to their polarization before they are split by the red optical couplers using the half-wave plate. After this step, signals are cross-coupled into the four SOAs by green optical couplers. The FWM effect occurs in the SOAs. The conjugate signal and the satellite signal, the generated FWM components, are only produced when the input signals have similar polarization states. Otherwise, the output of SOAs will produce no signals. After transmission of SOAs, the signals are filtered by tunable filters (TF), and the conjugate signal remains. In the end, the output DMUX can be observed. In this setup, we use polarization control (PC) to control the relative polarization state between two signals. The SOA region is the most prominent section of this setup because it functions both as an optical conjugator and an optical amplifier.

In our simulation, we assume that the polarization vectors of the input PolSK signals are parallel to the principal axes of the SOA, and correspond with the TE and TM modes. In our model, we also assume that the input waves are linearly polarized in the same direction. The coupled-wave equations of the input and output signals for the TE or TM mode in the subsection, respectively, can be expressed as[1,4]

$$\begin{aligned}\frac{\mathrm{d}A_{\mathrm{s1},i}}{\mathrm{d}z} =& \frac{1}{2}\left[\frac{\Gamma g_{\mathrm{s1},i}}{1+P_i/P_{\mathrm{s}}}(1-i\alpha_i)-\alpha_i\right]A_{\mathrm{s1},i} \\ &- \frac{\Gamma g_{\mathrm{s1},i}}{2(1+P_i/P_{\mathrm{s}})}(\eta_{\mathrm{s1,s2}}|A_{\mathrm{s2},i}|^2 \\ &+ \eta_{\mathrm{s1,c}}|A_{\mathrm{c},i}|^2+\eta_{\mathrm{s1,sat}}|A_{\mathrm{sat},i}|^2)A_{\mathrm{s1},i} \\ &- \frac{\Gamma g_{\mathrm{s1},i}}{2(1+P_i/P_{\mathrm{s}})}[(\eta_{\mathrm{s2,s1}}+\eta_{\mathrm{c,s1}})A_{\mathrm{s2},i}A_{\mathrm{c},i}A^*_{\mathrm{sat},i} \\ &+ \eta_{\mathrm{s2,sat}}A^2_{\mathrm{s2},i}A^*_{\mathrm{sat},i}],\end{aligned} \quad (1)$$

$$\begin{aligned}\frac{\mathrm{d}A_{\mathrm{s2},i}}{\mathrm{d}z} =& \frac{1}{2}\left[\frac{\Gamma g_{\mathrm{s2},i}}{1+P_i/P_{\mathrm{s}}}(1-i\alpha_i)-\alpha_i\right]A_{\mathrm{s2},i} \\ &- \frac{\Gamma g_{\mathrm{s2},i}}{2(1+P_i/P_{\mathrm{s}})}(\eta_{\mathrm{s2,s1}}|A_{\mathrm{s1},i}|^2 \\ &+ \eta_{\mathrm{s1,c}}|A_{\mathrm{c},i}|^2+\eta_{\mathrm{s1,sat}}|A_{\mathrm{sat},i}|^2)A_{\mathrm{s2},i} \\ &- \frac{\Gamma g_{\mathrm{s2},i}}{2(1+P_i/P_{\mathrm{s}})}[(\eta_{\mathrm{s1,s2}}+\eta_{\mathrm{sat,s2}})A_{\mathrm{s2},i}A_{\mathrm{c},i}A^*_{\mathrm{s1},i} \\ &+ \eta_{\mathrm{s2,c}}A^2_{\mathrm{s1},i}A^*_{\mathrm{c},i}],\end{aligned} \quad (2)$$

$$\begin{aligned}\frac{\mathrm{d}A_{\mathrm{c},i}}{\mathrm{d}z} =& \frac{1}{2}\left[\frac{\Gamma g_{\mathrm{c},i}}{1+P_i/P_{\mathrm{s}}}(1-i\alpha_i)-\alpha_i\right]A_{\mathrm{c},i} \\ &- \frac{\Gamma g_{\mathrm{c},i}}{2(1+P_i/P_{\mathrm{s}})}(\eta_{\mathrm{c,s1}}|A_{\mathrm{s1},i}|^2 \\ &+ \eta_{\mathrm{s1,c}}|A_{\mathrm{s2},i}|^2+\eta_{\mathrm{s1,sat}}|A_{\mathrm{sat},i}|^2)A_{\mathrm{c},i} \\ &- \frac{\Gamma g_{\mathrm{c},i}}{2(1+P_i/P_{\mathrm{s}})}[(\eta_{\mathrm{s2,sat}}+\eta_{\mathrm{s1,sat}})A_{\mathrm{s1},i}A_{\mathrm{s2},i}A^*_{\mathrm{sat},i} \\ &+ \eta_{\mathrm{s1,s2}}A^2_{\mathrm{s1},i}A^*_{\mathrm{s2},i}],\end{aligned} \quad (3)$$

$$\begin{aligned}\frac{\mathrm{d}A_{\mathrm{sat},i}}{\mathrm{d}z} =& \frac{1}{2}\left[\frac{\Gamma g_{\mathrm{sat},i}}{1+P_i/P_{\mathrm{s}}}(1-i\alpha_i)-\alpha_i\right]A_{\mathrm{sat},i} \\ &- \frac{\Gamma g_{\mathrm{sat},i}}{2(1+P_i/P_{\mathrm{s}})}(\eta_{\mathrm{sat,s1}}|A_{\mathrm{s1},i}|^2 \\ &+ \eta_{\mathrm{s1,c}}|A_{\mathrm{s2,i}}|^2+\eta_{\mathrm{s1,sat}}|A_{\mathrm{c},i}|^2)A_{\mathrm{sat}} \\ &- \frac{\Gamma g_{\mathrm{sat},i}}{2(1+P_i/P_{\mathrm{s}})}[(\eta_{\mathrm{s2,c}}+\eta_{\mathrm{s1,c}})A_{\mathrm{s1},i}A_{\mathrm{s2},i}A^*_{\mathrm{c},i} \\ &+ \eta_{\mathrm{s2,s1}}A^2_{\mathrm{s2},i}A^*_{\mathrm{s1},i}].\end{aligned} \quad (4)$$

In these equations, $g_{j,i}$ is the material gain coefficient of the SOA; $A_i = A_i(z,t)$, $j = s_1$; and s_2, c, and sat are the quasi-steady-state evolution of the probe, pump, and signal wave amplitudes, respectively. Here, P_{i} is the total optical power inside subsection i; P_{s} is the saturation power; α is the linewidth enhancement factor; α_{l} is the internal loss of SOA; and Γ is the confinement factor. The coefficients $\eta_{j,j'}$, $j \neq j'$, $j = s_1$, s_2, c, and sat represent the nonlinear interactions among the mixing waves. It can be decomposed to the three different segments from the nonlinear processes considered: the carrier density pulsations (CDP), the carrier heating (CH), and the

Table 1. Parameters Used in the Simulation

Symbol	Parameter	Value
L	Length of Active Region (m)	1×10^{-3}
W	Width of Active Region (m)	3.3×10^{-6}
D	Thickness of Active Region (m)	0.15×10^{-6}
C_1	Nonradiative Recombination Coefficient (s^{-1})	1.5×10^{8}
C_2	Bimolecular Recombination Coefficient ($\mathrm{m}^3\cdot\mathrm{s}^{-1}$)	2.5×10^{-17}
C_3	Auger Recombination Coefficient ($\mathrm{m}^6\cdot\mathrm{s}^{-1}$)	9.4×10^{-41}
α_l	Internal Loss of SOA (m^{-1})	4×10^{3}
Γ	Optical Confinement Factor	0.3
N	Refractive Index	3.22
P_{sat}	Saturation Power (W)	1.0×10^{-2}
α_{CH}	Line width Enhancement Factor by CH	3.6
α_{SHB}	Line width Enhancement Factor by SHB	0.1
$\varepsilon_{\mathrm{CH}}$	Carrier Heating Parameter (W^{-1})	4
$\varepsilon_{\mathrm{SHB}}$	Spectral Hole Burning Parameter (W^{-1})	6
T_s	Carrier Lifetime (s)	1.6×10^{-10}
T_1	Carrier Heating Time (s)	6.5×10^{-13}
T_2	Spectral-hole Burning Time (s)	1.0×10^{-13}
m_{c}	Effective Mass of Electron in the CB (kg)	4.10×10^{-32}
m_{hh}	Effective Mass of a Heavy Hole in the VB (kg)	4.19×10^{-31}
m_{lh}	Effective Mass of Electron in the CB (kg)	5.06×10^{-32}

spectral hole burning (SHB)[9]. All parameters used in these equations are shown in Table 1. To calculate each signal wave amplitude, the total signal wave amplitude is divided into m segments.

The material gain at a certain frequency (v) is given as the difference between the stimulated emission and absorption rates between the conduction and valance bands. Basically, the gain is given as a product of three terms: the density of states in the conduction and valance bands, the transition probability $|M|^2$, and the probabilities for having states occupied given by the Fermi-Dirac distribution. As a result, the material gain, $\mathrm{g_m}(\mathrm{m}^{-1})$, is given by[9]

$$\mathrm{g}(v,N)=\frac{e^2|M|^2}{4\pi^2\varepsilon_0 m_0^2 c n_\mathrm{g} v}\left[\frac{8\pi^2 m_\mathrm{e} m_\mathrm{hh}}{h^2(m_\mathrm{e}+m_\mathrm{hh})}\right]^{3/2} \cdot (hv-E_\mathrm{g})^{1/2}[f_\mathrm{c}(v)+f_\mathrm{v}(v)-1], \qquad (5)$$

where h is the Plancks constant, ε_0 is the vacuum permittivity, N is the carrier density, $|M|^2$ is the momentum matrix element, E_g is the band-gap energy, and f_c and f_v are the Fermi-Dirac distributions for the conduction and valence bands, respectively. In addition, m_e and m_hh represent the conduction band (CB) electron and the valence band (VB) heavy-hole effective masses, respectively.

The carrier density in section i is described by the following rate equation in the semiconductor optical amplifier when a current I is applied as

$$\begin{aligned}\frac{\mathrm{d}N_i}{\mathrm{d}t}&=\frac{1}{ewdL}-(C_1N_i+C_2N_i^2+C_3N_i^2)\\&-\sum_{j=s_1,s_2,c,\mathrm{sat}} g_{j,i}\frac{G_{j,i}-1}{\ln G_{j,i}}\frac{|A_{j,i}|^2\lambda_j}{hcw\mathrm{d}}\\&-\sum_{j=1}^{m} g_{j,i}\frac{2g_{j,i}}{\overline{g}_{j,i}}\left(\frac{G_{j,i}-1}{\ln G_{j,i}}-1\right)\\&+\frac{G_{j,i}-1}{\ln G_{j,i}}\frac{\Delta\lambda(w_{j,i}^{+}+w_{j,i}^{-})\lambda_j}{hcwd},\end{aligned} \qquad (6)$$

where I is the injection current, the injected current that produces gain in the gain region; wdL is the volume of the active region; $w_{j,i}(z,t)$ is the power spectrum density; c_1 is the nonradiative recombination coefficient; c_2 is the bimolecular recombination coefficient; and c_3 is the Auger recombination coefficient . In addition, $G_{j,i}=\exp(\overline{g}_{j,i}\Delta 1)$ is the gain of subsection i. The third and fourth terms on the right-hand side are the carrier consumptions induced by the stimulated emissions for the signals, including the conjugate signal, the satellite signal, and the ASE. In order to analyze the four SOAs, we use the FDM based on solving traveling wave equations. The typical values of the parameters used in the simulations are shown in Table 1.

In our simulation, we use input signals with peak power 20 mW. The duration of each of input pulse to the SOA is 25 ps, as shown in the left-side SOA. The coupling coefficient of all couplers is 0.5. The central wavelengths of the two input signals are 1 550 and 1 551 nm, respectively. The performance of each signal is analyzed numerically by the FDM method. The typical values of the parameters used in our simulation are shown in Table 1.

In the numerical model, the amplifier is split into a number of sections, labeled $i = 1$ to N_z, as shown in Fig. 3. The signal fields and spontaneous emission photon rates are estimated at the section interfaces. Forward differences are used for positive traveling waves, and backward differences are used for negative traveling waves. If E^+ is a forward-traveling wave, then, for the ith section, the spatial derivative is approximated by

$$\frac{\mathrm{d}E^+}{\mathrm{d}z}=\frac{E_i-E_{i-1}}{\Delta z}.$$

Similarly, if E^- is a backward-traveling wave, then, for the ith section, the spatial derivative is approximated by

$$\frac{\mathrm{d}E^-}{\mathrm{d}z}=\frac{E_{i+1}-E_i}{\Delta z},$$

where $\Delta z = L/N_\mathrm{z}$ is the length of a single section.

Several material gain coefficients responding to different carrier densities are calculated as a function of wavelength, as illustrated in Fig. 4(a). It clearly shows that, with the carrier density increasing, the output of the material gain coefficient increases. This topic is very important in our calculations and should be specifically noted. At low input powers, the carrier density has symmetrical spatial distribution, peaking at the center of the SOA, and tailing off toward the input and output facets, as shown in Fig. 4(b).

Figure 5 shows the all-optical DMUX time diagram for length of SOA $L = 1\,000$ μm and injection current of

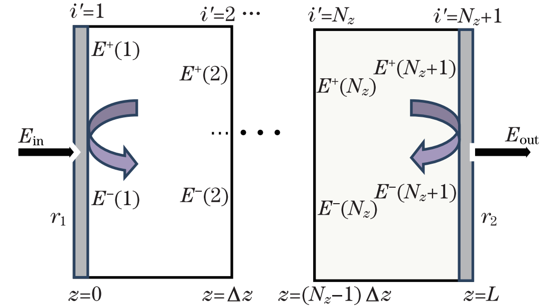

Fig. 3. Sections of the SOA model. Signal fields are estimated at the section boundaries. The carrier density is estimated at the center of the section.

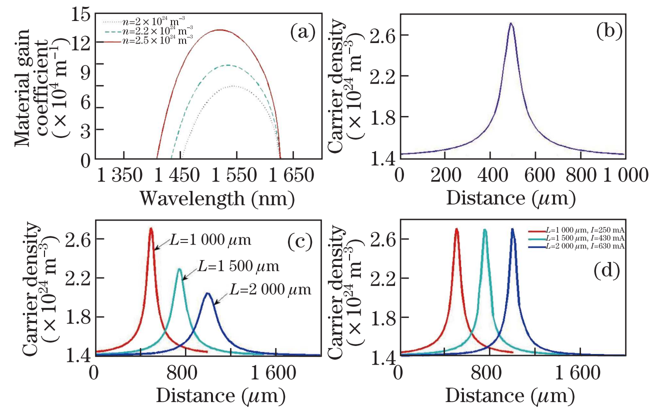

Fig. 4. (a) Typical InGaAsP bulk semiconductor material gain coefficient spectra for several carrier density measurements; (b) SOA carrier density.

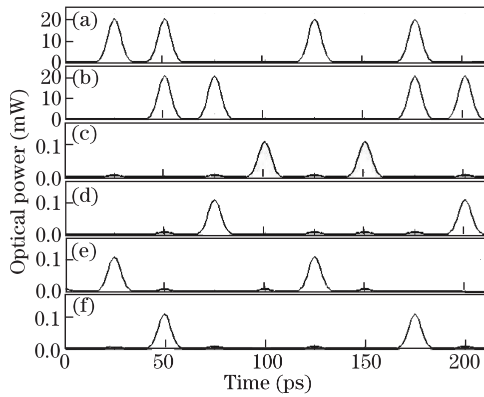

Fig. 5. Intensity waveforms for (a) input signal 1, (b) input signal 2, (c) y_0 output, (d) y_1 output, (e) y_2 output, and (f) y_3 output.

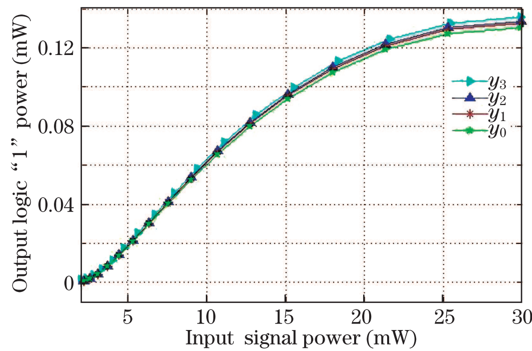

Fig. 6. Output power levels of logic "1" of all-optical DMUX as a function of input signal 1 power.

250 mA under $\Gamma^{\mathrm{TE}} = \Gamma^{\mathrm{TM}} = 0.3$. Figure 5 clearly shows that the peak power of the output signals is approximately 0.11 mW.

Figure 6 shows the output power levels of logic "1" of the all-optical DMUX as a function of the input signal "1" power with length of SOA L= 1 000 μm and bias of I = 250 mA. Figure 5 clearly shows that the power of the conjugate signal increases with the increase of the signal "1" power. The power of the signal "1" cannot be too small because, in this state, the power of the conjugate signal would be too small and useless.

We then repeat our simulation for several different lengths of the SOA section[3]. The results are shown in Figs. 4(c) and (d). In order to improve the output power level of the logic "1," we find that the output power level of logic "1" increases with the injection current and length of the SOA section. Figure 4(c) shows the carrier density with length of SOA ($L = 1\,000$ μm, $L = 1\,500$ μm, and $L = 2\,000$ μm) and bias current of $I = 250$ mA. Figure 4(c) clearly shows that, as the length of SOA section increases from 1 000 μm to 2 000 μm, the carrier density decreases. By correctly selecting the injection current, we are able to compensate for this decreasing of carrier density. Figures 4(d) and 7 show the carrier density and the output power levels of logic "1" of the all-optical DMUX as a function of input signal "1" power, respectively, with SOA length of $L = 1\,000$ μm and bias of $I = 250$ mA, SOA length of $L = 1\,500$ μm and bias of $I = 430$ mA, and SOA length of $L = 2\,000$ μm and bias of $I = 630$ mA.

Figure 7 shows that, with the SOA section and bias current increasing, the optical output power increases. However, we must note that this bias current injection increase could be injurious to the device. We must thus find another way to improve the optical output power. One crucial parameter in the SOA design is the radiation confinement factor Γ, which is defined as the fraction of the mode energy confined to the active layer[10]:

$$\Gamma = \frac{\int_z |\langle s_z(x,y)\rangle| \mathrm{d}x\mathrm{d}y}{\int_{-\infty}^{+\infty} |\langle s_z(x,y)\rangle| \mathrm{d}x\mathrm{d}y}, \tag{7}$$

where $\langle s_z(x,y)\rangle$ is the time-averaged z-component of the Poynting vector, and the integral in the numerator is over the ith layer. Currently one can obtain Γ values for $\mathrm{In}_{1-x}\mathrm{Ga}_x\mathrm{As}_y\mathrm{P}_{1-y}$ double heterostructures by using the numerically calculated plots of Γ versus d for several values of $\Delta n = n_1 - n_2$ in Fig. 8(a), where n_1, n_2 are the indices of refraction of the active and cladding layers, respectively, and d is the thickness of the active layer (see Ref. [11]).

The choice of materials for semiconductor amplifiers is principally determined by the requirement that the probability of radiative recombination should be sufficiently high to ensure sufficient gain at low current. The output power level of logic "1" can be improved by increasing the optical confinement factor. Figure 8 shows that, by increasing the active layer thickness, the confinement factor is increased. Therefore, the output power level of logic "1" can be improved by increasing the active layer thickness. However, we should note that this increase of the active layer thickness decreases the carrier density, as shown in Eq. (6). By correctly selecting the injection current, we can observe this decreasing of the carrier

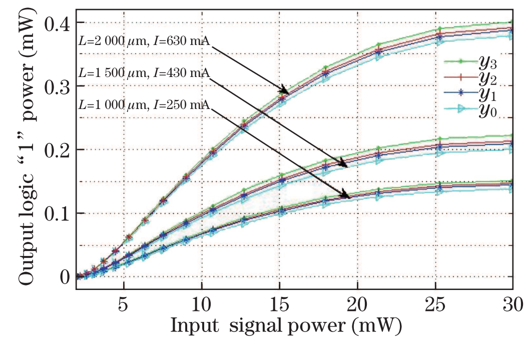

Fig. 7. Output power levels of logic "1" of all-optical DMUX as a function of input signal 1 power.

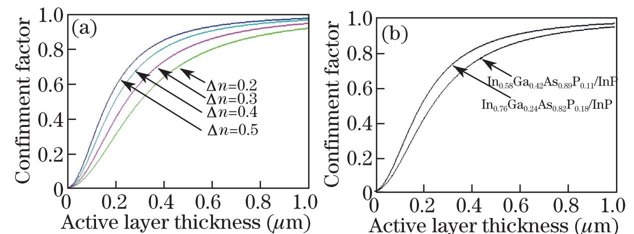

Fig. 8. (a) Optical confinement factor as a function of thickness of active layer for several values of Δn; (b) comparison of numerically calculated optical confinement factor for $\mathrm{In_{0.58}Ga_{0.42}As_{0.89}P_{0.11}}$ and $\mathrm{In_{0.76}Ga_{0.24}As_{0.82}P_{0.18}}$ device.

density. Figure 8 also shows that the conversion of the molar fractions of arsenide and gallium can improve the confinement factor.

We repeat our simulation for the InP-$In_{0.76}Ga_{0.24}As_{0.82}P_{0.18}$ device and investigate effects of this device substance conversion on the optical output power. All material parameters for InP-$In_{0.76}Ga_{0.24}As_{0.82}P_{0.18}$ under consideration were reported in Ref. [12]. With this work, the confinement factor will increase. For example, with length of SOA $L = 1\,000$ μm, thickness of active layer 0.2 μm, injection current 290 mA, the confinement factor for InP-$In_{0.76}Ga_{0.24}As_{0.82}P_{0.18}$ device increases to 0.48. Therefore, the peak power of the conjugate signal or output power level of logic "1" increases to more than twice that in the previous state (InP-$In_{0.58}Ga_{0.42}As_{0.89}P_{0.11}$ device), or approximately 0.27 mW, for the peak power of the output signals.

In conclusion, a novel scheme for ultrafast all-optical DMUX based on FWM in SOA is proposed in this letter. We present a comprehensive polarization-dependent broadband model of the ultrafast all-optical DMUX and investigate the performance at 40 Gb/s. We use a finite-difference method to analyze the behavior of four SOA sections. The four output fields, A_i, $i = s_1$, s_2, c, and sat are calculated numerically. In general, for the thickness of active layer range, higher active layer thickness can increase the output power levels of logic "1"[13]. The carrier density decreases as the active layer thickness increases. By correctly selecting the injection current, we can correct this decrease of the carrier density. A tradeoff between large output powers and power consumption occurs. We also study the relation between optical confinement factor and thickness of active layer of the SOA section, and investigate effect of confinement factor increasing on the optical output power. This scheme has the potential for application in future high-bit-rate optical networks.

References

1. P. Li, D. Huang, and X. Zhang, IEEE J. Quantum Electron. **45,** 1542 (2009).
2. Hassan Kaatuzian, *Photonics* (Amirkabir University of Technology PRESS, Tehran, 2009) vol. 2.
3. H. Ahmadi and H. Kaatuzian, in *Proceedings of IEEE International Workshop on Nonlinear Photonics Conference* (*NLP-LFNM*) *Ukraine* (2011).
4. P. Li, D. Huang, X. Zhang, and G. Zhu, Opt. Express **14,** 11839 (2006).
5. Z, Li and G. Li, IEEE Photon. Technol. Lett. **18,** 1341 (2006).
6. V. Sharma, S. S. Pattnaik, S. Devi, S. Kamal, T. Garg, A. Pathak, and M. Smriti, J. Electrial Electron. Eng. Res. **2,** 68 (2010).
7. M. J. Connelly, IEEE J. Quantum Electron. **37,** 439 (2001).
8. H. Kaatuzian and M. K. Moazzam, Opt. Eng. **47,** 014202 (2008).
9. B. Mikkelson, "Optical amplifier and their system applications", PhD. Thesis (Denmark Univ. Technol., Lyngby, Denmark, 1994).
10. T. D. Visser, H. Blok, and B. Demeulenaere, IEEE J. Quantum Electron. **33,** 1763 (1997).
11. D. Botez, IEEE J. Quantum Electron. **QE-14,** 230 (1978).
12. J. Piprek, D. I. Babic, and J. E. Bowers, J. Appl. Phys. **81,** 15 (1997).
13. H. Ahmadi and H. Kaatuzian, in *Proceedigns of IEEE High-Capacity Optical Network & Emerging/Enabling Technologies conference* (*HONET*) *Riyadh, Saudi Arabia* (2011).